

# Integrated Sachs-Wolfe tomography with orthogonal polynomials

Gero Jürgens<sup>\*1</sup> and Björn Malte Schäfer<sup>2</sup>

<sup>1</sup>*Institut für theoretische Astrophysik, Zentrum für Astronomie, Universität Heidelberg, Albert-Ueberle-Straße 2, 69120 Heidelberg, Germany*

<sup>2</sup>*Astronomisches Recheninstitut, Zentrum für Astronomie, Universität Heidelberg, Mönchhofstraße 12, 69120 Heidelberg, Germany*

13 November 2018

## ABSTRACT

Topic of this article are tomographic measurements of the integrated Sachs-Wolfe effect with specifically designed, orthogonal polynomials which project out statistically independent modes of the galaxy distribution. The polynomials are constructed using the Gram-Schmidt orthogonalisation method. To quantify the power of the iSW-effect in constraining cosmological parameters we perform a combined Fisher matrix analysis for the iSW-, galaxy- and cross-spectra for  $w$ CDM cosmologies using the survey characteristics of PLANCK and EUCLID. The signal to noise ratio has also been studied for other contemporary galaxy surveys, such as SDSS, NVSS and 2MASS. For the cross-spectra our tomographic method provides a 16% increase in the signal to noise ratio and an improvement of up to 30% in conditional errors on parameters. Including all spectra, the marginalised errors approach an inverse square-root dependence with increasing cumulative polynomial order which underlines the statistical independence of the weighted signal spectra.

**Key words:** cosmology: large-scale structure, integrated Sachs-Wolfe effect, methods: analytical

## 1 INTRODUCTION

The integrated Sachs-Wolfe (iSW) effect is one of the secondary anisotropies of the cosmic microwave background (CMB). Time-evolving gravitational potentials in the large-scale structure generate temperature fluctuations in the CMB (Sachs & Wolfe 1967). The iSW-effect is a valuable tool for investigating dark energy and non-standard cosmologies since it is sensitive to fluids with non-zero equation of state (Crittenden & Turok 1996). For this reason its detection is of particular relevance for cosmology and the nature of gravity (Lue et al. 2004; Zhang 2006) even if its signal strength is very low.

Since the iSW-effect is generated in time-evolving potential wells for photons on their way from the last scattering surface to us, it will be strongly correlated with the galaxy density field. Therefore, the cross-spectrum will provide valuable additional cosmological information. The iSW effect has been measured in such cross-correlation studies (Boughn et al. 1998; Boughn & Crittenden 2004; Vielva et al. 2006; McEwen et al. 2007; Giannantonio et al. 2008). However, due to the line of sight integration, a detailed distance resolution of the processes can not be withdrawn from these spectra.

A former approach correlated large scale structure observations from various survey with the CMB anisotropies to study the iSW-effect as a function of redshift and to formulate a reliable likelihood formulation for parameter constraints (Ho et al. 2008). Also recently, Frommert et al. (2008) presented an optimal method to re-

duce the local variance effect and gained 7 per cent in the signal to noise ratio for the cross-spectra.

In this work we aim to formulate a tomographic approach with help of an orthogonal set of weighting polynomials, which is similar to a former application to weak lensing spectra (Schaefer & Heisenberg 2011). The orthogonality of the polynomials will generically lead to a diagonal signal covariance matrix and will therefore provide cumulative statistical independent measurements with increasing polynomial order.

The article has the following structure: In Section 2 we provide introductory information about dark energy cosmologies, CDM power spectra and linear structure growth within these cosmologies (Sections 2.1-2.3). We also introduce a galaxy distribution function (Section 2.4) and give a short introduction to the iSW-effect (Section 2.5). The orthogonal polynomials are motivated and constructed in Section 3.1 and 3.2, also their most important properties are discussed (Section 3.3). In Section 4 we discuss how tomography with orthogonal polynomials can improve statistical constraints on cosmological parameters. After calculating the noise contributions (Section 4.1) we perform a Fisher matrix analysis (Section 4.2) and discuss signal to noise ratios and statistical errors (Section 4.3-4.4). The results are summarised in Section 5.

The reference cosmological model used is a spatially flat  $w$ CDM cosmology with Gaussian adiabatic initial perturbations in the cold dark matter density field. The specific parameter choices are  $\Omega_m = 0.25$ ,  $n_s = 1$ ,  $\sigma_8 = 0.8$ ,  $\Omega_b = 0.04$  and  $H_0 = 100 h$  km/s/Mpc, with  $h = 0.72$ . The dark energy equation of state is set to  $w = -0.9$  and the sound speed is equal to the speed of light,  $c_s = c$ .

\* gero.juergens@stud.uni-heidelberg.de

## 2 COSMOLOGY AND ISW-EFFECT

### 2.1 Dark energy cosmologies

In spatially flat dark energy cosmologies with the matter density parameter  $\Omega_m$ , the Hubble function  $H(a) = d \ln a / dt$  is given by

$$\frac{H^2(a)}{H_0^2} = \Omega_m a^{-3} + (1 - \Omega_m) a^{-3(1+w)}, \quad (1)$$

with a constant dark energy equation of state parameter  $w$ . The value  $w \equiv -1$  corresponds to the cosmological constant  $\Lambda$ . The relation between comoving distance  $\chi$  and scale factor  $a$  is given by

$$\chi = c \int_a^1 da \frac{1}{a^2 H(a)}, \quad (2)$$

in units of the Hubble distance  $\chi_H = c/H_0$ .

### 2.2 CDM power spectrum

The linear CDM density power spectrum  $P(k)$  describes the fluctuation amplitude of the Gaussian homogeneous density field  $\delta$ ,  $\langle \delta(\mathbf{k}) \delta^*(\mathbf{k}') \rangle = (2\pi)^3 \delta_D(\mathbf{k} - \mathbf{k}') P(k)$ , and is given by the ansatz

$$P(k) \propto k^{ns} T^2(k), \quad (3)$$

with the transfer function  $T(k)$ . In low- $\Omega_m$  cosmologies  $T(k)$  is approximated with the fit proposed by Bardeen et al. (1986),

$$T(q) = \frac{\ln(1 + 2.34 q)}{2.34 q} \times \left[ 1 + 3.89 q + (16.1 q)^2 + (5.46 q)^3 + (6.71 q)^4 \right]^{-1/4} \quad (4)$$

where the wave number  $k = q\Gamma$  is rescaled with the shape parameter  $\Gamma$  (Sugiyama 1995) which assumes corrections due to the baryon density  $\Omega_b$ ,

$$\Gamma = \Omega_m h \exp \left[ -\Omega_b \left( 1 + \frac{\sqrt{2h}}{\Omega_m} \right) \right]. \quad (5)$$

The spectrum  $P(k)$  is normalised to the variance  $\sigma_8$  on the scale  $R = 8 \text{ Mpc}/h$ ,

$$\sigma_R^2 = \frac{1}{2\pi^2} \int dk k^2 P(k) W^2(kR) \quad (6)$$

with a Fourier transformed spherical top hat filter function,  $W(x) = 3j_1(x)/x$ .  $j_\ell(x)$  is the spherical Bessel function of the first kind of order  $\ell$  (Abramowitz & Stegun 1972).

### 2.3 Structure growth with clustering dark energy

Linear homogeneous growth of the density field,  $\delta(\mathbf{x}, a) = D_+(a)\delta(\mathbf{x}, a=1)$ , is described by the growth function  $D_+(a)$ , which is the solution to the growth equation (Turner & White 1997; Wang & Steinhardt 1998; Linder & Jenkins 2003),

$$\frac{d^2}{da^2} D_+(a) + \frac{1}{a} \left( 3 + \frac{d \ln H}{d \ln a} \right) \frac{d}{da} D_+(a) = \frac{3}{2a^2} \Omega_m(a) D_+(a). \quad (7)$$

### 2.4 Galaxy distribution

Galaxies form when strong peaks in the density field decouple from the Hubble expansion due to self-gravity. These so called protohalos approximately undergo an elliptical collapse (Mo et al. 2007; Sheth et al. 2001).

In contrary to the pressureless dark matter component the baryons inside a dark matter halo can loose energy via radiative cooling and form stars. Because of this different behaviour, strictly speaking, one can not deduce the fractional perturbation  $\Delta n / \langle n \rangle$  in the mean number density of galaxies  $\langle n \rangle$  from the dark matter overdensity  $\delta = \Delta \rho / \rho$ . In a very simple way, however, the linear relation between the two entities,

$$\frac{\Delta n}{\langle n \rangle} = b \frac{\Delta \rho}{\langle \rho \rangle}, \quad (8)$$

is a good approximation in most cases and was proposed by Bardeen et al. (1986). The bias parameter  $b$  can generally depend on scale (Lumsden et al. 1989), time (Fry 1996; Tegmark & Peebles 1998) as well as the galaxies luminosity and morphology. For simplicity we set the galaxy bias to unity throughout this paper,  $b \equiv 1$ . An established parametrisation of the redshift distribution  $n(z) dz$  of galaxies is

$$n(z) dz = n_0 \left( \frac{z}{z_0} \right)^2 \exp \left[ - \left( \frac{z}{z_0} \right)^\beta \right] dz \quad \text{with} \quad \frac{1}{n_0} = \frac{z_0}{\beta} \Gamma \left( \frac{3}{\beta} \right) \quad (9)$$

which was introduced by Smail et al. (1995) and will also be used in this work. The parameter  $z_0$  is related to the median redshift of the galaxy sample  $z_{\text{med}} = 1.406 z_0$  if  $\beta = 3/2$ . Finally, the  $\Gamma$ -function (Abramowitz & Stegun 1972) determines the normalisation parameter  $n_0$ .

### 2.5 The integrated Sachs-Wolfe (iSW) effect

Due to its expansion our universe had cooled down sufficiently to allow the formation of hydrogen atoms at a redshift of  $z \approx 1089$  (Spergel et al. 2003). Fluctuations in the gravitational potential imposed a shift in the decoupled photons which were emitted in the (re)combination process (Sachs-Wolfe effect). This primary anisotropy can be observed in the cosmic microwave background (CMB) in form of temperature fluctuations  $\Delta T / T_{\text{CMB}} \approx 10^{-5}$  on large scales around its mean temperature  $T_{\text{CMB}} = 2.726 \text{ K}$  (Fixsen 2009).

Besides this, photons are subjected to several other effects on their way to us, which lead to secondary anisotropies (Aghanim et al. 2008), of which only the most important ones are mentioned here: Gravitational lensing (Bartelmann & Schneider 2001), Compton-collisions with free cluster electrons (Sunyaev-Zeldovich effect, Zeldovich & Sunyaev 1980) and with electrons in uncollapsed structures (Ostriker-Vishniac effect, Ostriker & Vishniac 1986) and gravitational coupling to linear time-evolving potential wells (integrated Sachs-Wolfe effect, Sachs & Wolfe 1967, which will be subject of this work).

Assuming a completely transparent space, i.e. vanishing optical depth due to compton scattering  $\tau_{\text{opt}}(\eta) = 0$ , the temperature fluctuations  $\tau(\theta)$  generated by the iSW-effect can be expressed by the line of sight integral (Sachs & Wolfe 1967)

$$\tau(\theta) \equiv \frac{\Delta T_{\text{iSW}}}{T_{\text{CMB}}} = \frac{2}{c^3} \int_0^{\chi_H} d\chi a^2 H(a) \frac{\partial}{\partial a} \Phi(\theta\chi, \chi), \quad (10)$$

reaching out to the limit of Newtonian gravity. Using the Poisson equation we can write this integral in terms of the dimensionless potential  $\phi = \Phi/\chi_H^2 = \Delta^{-1} \delta/\chi_H^2$  from the density field  $\delta$ :

$$\tau(\theta) = \frac{3\Omega_m}{c} \int_0^{\chi_H} d\chi a^2 H(a) \frac{d}{da} \frac{D_+}{a} \phi(\theta\chi, \chi). \quad (11)$$

Heuristically, the effect originates from an unbalance between the

photon's blue-shift when entering a time varying potential well and the red-shift experienced at the exit.

The effect vanishes identically in matter dominated universes  $\Omega_m = 1$ , since then  $D_+/a$  is a constant. Therefore, a non-zero iSW-signal will be an indicator of a cosmological fluid with  $w \neq 0$ . After the radiation dominated era it will thus be a valuable tool for investigating dark energy cosmologies.

Since the inverse Laplacian which solves for the potential in the Poisson equation introduces a  $k^{-2}$  term, small scale fluctuations will be quadratically damped. For this reason the iSW-effect provides a signal on large scales and will be negligible above  $\ell \approx 100$ .

In order to identify the sources of the effect it is sensible to investigate the cross correlation of the iSW amplitude with the line of sight projected galaxy density  $\gamma$ :

$$\gamma(\boldsymbol{\theta}) = b \int_0^{\chi_H} d\chi n(z) \frac{dz}{d\chi} D_+ \delta(\boldsymbol{\theta}, \chi). \quad (12)$$

We obtain the dimensionless observables  $\gamma$  and  $\tau$  from a line of sight integration of the two dimensionless source fields  $\delta$  and  $\phi$  weighted by functions which carry units of inverse length.

If one is interested in rather small scales one can approximate the sphere locally as being plane and perform a Fourier transform

$$\gamma(\boldsymbol{\ell}) = \int d^2\theta \gamma(\boldsymbol{\theta}) e^{-i(\boldsymbol{\ell} \cdot \boldsymbol{\theta})}. \quad (13)$$

Clearly, there is no directional dependence,  $\gamma(\boldsymbol{\ell}) = \gamma(\ell)$ , and one can define the spectrum  $C_{\gamma\gamma}(\ell)$ :

$$\langle \gamma(\ell) \gamma^*(\ell') \rangle = (2\pi)^2 \delta_D(\ell - \ell') C_{\gamma\gamma}(\ell) \quad (14)$$

The observable  $\tau$  can be transformed in analogous way. With the two weighting functions

$$\begin{aligned} W_\gamma(\chi) &= n(z) \frac{H(z)}{c} D_+(z) \\ W_\tau(\chi) &= 3\Omega_m a^2 \frac{H}{c} \frac{d}{da} \frac{D_+}{a} \end{aligned} \quad (15)$$

we can now derive the spectra (Limber 1953),

$$\begin{aligned} C_{\gamma\gamma}(\ell) &= \int_0^{\chi_H} \frac{d\chi}{\chi^2} W_\gamma^2(\chi) P_{\delta\delta}(k = \ell/\chi) \\ C_{\tau\gamma}(\ell) &= \int_0^{\chi_H} \frac{d\chi}{\chi^2} W_\tau(\chi) W_\gamma(\chi) P_{\delta\phi}(k = \ell/\chi) \\ C_{\tau\tau}(\ell) &= \int_0^{\chi_H} \frac{d\chi}{\chi^2} W_\tau^2(\chi) P_{\phi\phi}(k = \ell/\chi). \end{aligned} \quad (16)$$

The power spectra can be related to the density power spectrum:

$$P_{\phi\phi}(k) = \frac{P_{\delta\delta}(k)}{(\chi_H k)^4}, \quad P_{\delta\phi}(k) = \frac{P_{\delta\delta}(k)}{(\chi_H k)^2}. \quad (17)$$

The multiplication factors  $k^{-2}$  and  $k^{-4}$  tilt the spectra to smaller values for increasing multipole order  $\ell$  and show once again the iSW-effect to be a large scale phenomenon.

### 3 TOMOGRAPHY WITH ORTHOGONAL POLYNOMIALS

#### 3.1 Motivation

Measurements of the iSW-effect provides integrated information about the structure formation history of our universe since the last scattering surface. Cross-correlation with the galaxy density field increases the signal to noise ratio significantly and the spectrum is noiseless due to uncorrelated noise in the CMB and the density

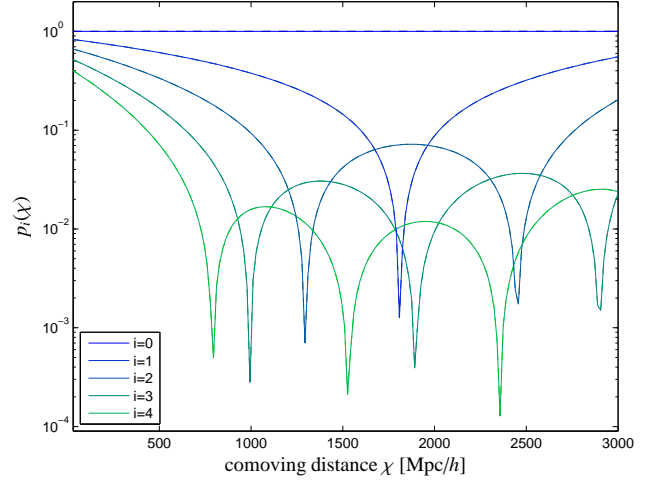


**Figure 1.** Orthogonal polynomials  $p_i(\chi)$ ,  $i = 0..4$ , as a function of comoving distance  $\chi$ . The lowest order polynomial is shown in blue, the highest order in green. The construction was performed with the Gram-Schmidt algorithm at multipole order  $\ell = 100$ .

field. However, due to the fact that both the cross-correlation spectrum and the galaxy spectrum are line of sight integrated quantities, non-linear effects of parameters on the signals could be averaged out and valuable tomographical information would be lost.

Tomographical methods split up the signal from different distances and are therefore able to increase the signal to noise ratio and the sensitivity with respect to cosmological parameters. In case of the galaxy spectra this implies that additional covariances between the different spectra have to be taken into account.

For a direct tomography in the line of sight integration of the iSW signal the knowledge of the large scale structure potential would be necessary. A reconstruction of the potential from the galaxy, however, would not reach the required accuracy.

To circumvent this issue we perform tomography in the galaxy signal and cross-correlate these with the iSW signal. In the course of this we are able to withdraw tomographical information also from the iSW signal. We use specifically designed polynomials for a distance weighting of the galaxy distribution. Defining the weighted galaxy covariances as a scalar product of the polynomials will lead to statistically independent galaxy spectra once the polynomials are orthogonalised. This nonlocal binning of the galaxies leads to a diagonalisation of the galaxy signal covariance matrix. The polynomials can then also be used for tomographical measurements in the iSW-galaxy cross-correlations.

#### 3.2 Construction of orthogonal sets of polynomials

Weighting the given galaxy distribution function  $n(\chi) = n(z) dz/d\chi = n(z) H(z)/c$  with a polynomial  $p_i(\chi)$  modifies the galaxy weighting function to

$$W_\gamma^{(i)}(\chi) = p_i(\chi) W_\gamma(\chi) = p_i(\chi) n(z) \frac{H(z)}{c} D_+(z). \quad (18)$$

For the polynomials  $p_i(\chi)$  and  $p_j(\chi)$  we require orthogonality

$$\langle p_i, p_j \rangle = 0 \text{ for } (i \neq j) \quad (19)$$

with respect to the following scalar product for the polynomials:

$$\langle p_i, p_j \rangle \equiv S_{\gamma\gamma}^{(ij)}(\ell) \equiv \int_0^{\chi_H} \frac{d\chi}{\chi^2} W_\gamma^{(i)}(\chi) W_\gamma^{(j)}(\chi) P(k = \ell/\chi). \quad (20)$$

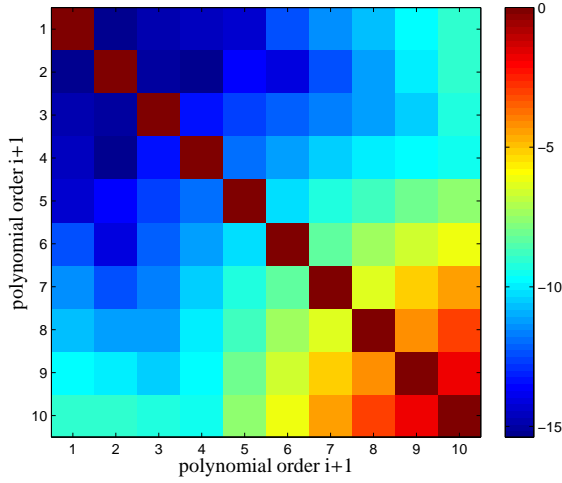


**Figure 2.** Numerical accuracy for the orthogonality relation  $\langle p_i, p_j \rangle$  at  $\ell = 20$  in logarithmic representation. The accuracy imposes a limit on the number of included polynomials.

The necessary properties for a scalar product are obviously fulfilled ( $\langle p_i, p_i \rangle \geq 0$ ,  $\langle p_i, p_i \rangle = 0 \Leftrightarrow p_i \equiv 0$  and linearity). We use the Gram-Schmidt procedure to construct orthogonal polynomials out of the family of monomials

$$p'_i(\chi) = \left( \frac{\chi}{\chi_{\text{node}}} \right)^i, \quad (21)$$

where  $\chi_{\text{node}}$  sets the position of the node of the first polynomial, which is in our case set to the median value of the redshift distribution. However, a change in  $\chi_{\text{node}}$  is completely absorbed in the coefficient and has no influence on the polynomials. Starting with the zero-order polynomial

$$p_0(\chi) = p'_0(\chi) \equiv 1, \quad (22)$$

the polynomials are constructed iteratively,

$$p_i(\chi) = p'_i(\chi) - \sum_{j=0}^{i-1} \frac{\langle p'_i, p_j \rangle}{\langle p_j, p_j \rangle} p_j(\chi). \quad (23)$$

The procedure has to be performed for every multipole  $\ell$ . The index  $\ell$  of the polynomials  $p_i(\chi)$  has been omitted for clarity. As one can see, the zero-order scalar product is equal to the galaxy spectrum:

$$\langle p_0, p_0 \rangle = S_{\gamma\gamma}(\ell). \quad (24)$$

Therefore, the unweighted case is already contained in the first weighting function. Finally, we can weight also the tracer density modes  $\gamma(\ell)$  themselves with a polynomial  $p_i(\chi)$

$$\gamma^{(i)}(\ell) = \int_0^{\chi_H} d\chi W_\gamma^{(i)}(\chi) \delta \quad (25)$$

for which a generalized version of the well known expression for the covariance holds in case of homogeneous and isotropic random fields:

$$\langle \gamma^{(i)}(\ell) \gamma^{(j)*}(\ell') \rangle = (2\pi)^2 \delta_D(\ell - \ell') S_{\gamma\gamma}^{(ij)}(\ell) \quad (26)$$

with  $S_{\gamma\gamma}^{(ij)}(\ell) \propto \delta_{ij}$ .

### 3.3 Properties of orthogonal polynomials

In Fig. 1 the orthogonal polynomials are shown up to a polynomial order of  $i = 4$ . They show an increasing number of zero points

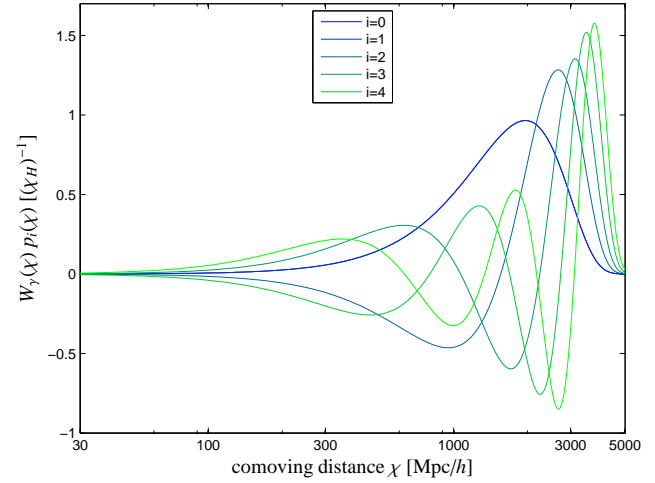


**Figure 3.** Weighted galaxy efficiency function  $W_\gamma^{(i)}(\chi)$ ,  $i = 0 \dots 4$ , as a function of comoving distance at multipole order  $\ell = 20$ .

roughly at the positions where the previous polynomial reaches a local maximum or minimum, which intuitively indicates their orthogonality.

As one can see in Fig. 2 orthogonality is fulfilled until numerical limitations become significant at a polynomial order of  $q \approx 9$ . The increasing numerical deviations from the orthogonality condition ( $\langle p_i, p_j \rangle = 0$  for  $i \neq j$ ) is due to the iterative method, which cumulates errors throughout the process. This implies the accuracy to shrink from  $10^{-15}$  for  $i = 0$  to  $10^{-3}$  for  $i = 8$ . This is a well known disadvantage of the Gram-Schmidt orthogonalisation method, especially when dealing with functions as opposed to vectors, since there is larger numerical noise in the evaluation of the scalar products. However, as we will later see, it is not necessary for our application to go to even higher orders.

In Fig. 3 the weighted galaxy efficiency functions  $W_\gamma^{(i)}(\chi)$  are depicted, which are modified by the polynomials  $p_i(\chi)$  at an angular scale of  $\ell = 19$ . The case  $i = 0$  refers to the weighting function without tomography,  $W_\gamma^{(0)}(\chi) = W_\gamma(\chi)$ . One can easily observe the order of the polynomial hierarchy at the high distance end of the functions, where one after another approaches zero.

The modified spectra  $C_{\gamma\gamma}^{(ii)}(\ell)$  and  $C_{\gamma\gamma}^{(i)}(\ell)$  are shown in Fig. 4 and Fig. 5, respectively. The drop in amplitude is mainly an effect of the absence of normalisation, while one can in fact observe slight differences in shape. However, these differences are small, since the polynomials only mildly depend on the multipole order  $\ell$ . Therefore, the overall shape of the spectra is still dominated by the zero-order spectra  $C_{\gamma\gamma}^{(00)}(\ell)$  and  $C_{\gamma\gamma}^{(0)}(\ell)$ , respectively. Thanks to the orthogonalisation these spectra now provide statistically independent information. In the next section we aim to combine signals from the galaxy distribution, the iSW-effect and the cross-spectra to investigate statistical bounds on cosmological parameters.

## 4 STATISTICS

This section aims to connect cosmic variance and statistical noise with the iSW-signal and its cross-correlations into a meaningful statistical formulation. In the course of this we construct covariance matrices for the polynomial-weighted spectra. Statistical errors on cosmological parameters are estimated in the Fisher-matrix formal-

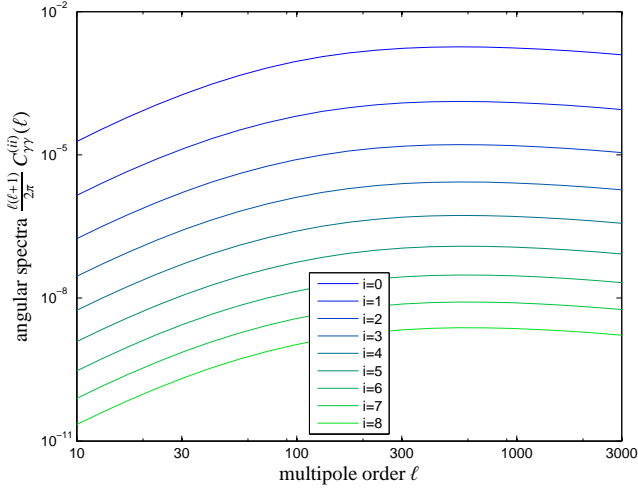


**Figure 4.** Pure galaxy-galaxy spectra  $S_{\gamma\gamma}^{(i)}(\ell)$ ,  $i = 0 \dots 8$ , weighted with orthogonal polynomials  $p_i(\chi)$ , as a function of the multipole order  $\ell$ .  $S_{\gamma\gamma}^{(00)}(\ell)$  (blue) refers to the non-tomographic spectrum  $S_{\gamma\gamma}(\ell)$ . One can see a decrease in amplitude for increasing multipole order  $\ell$ .

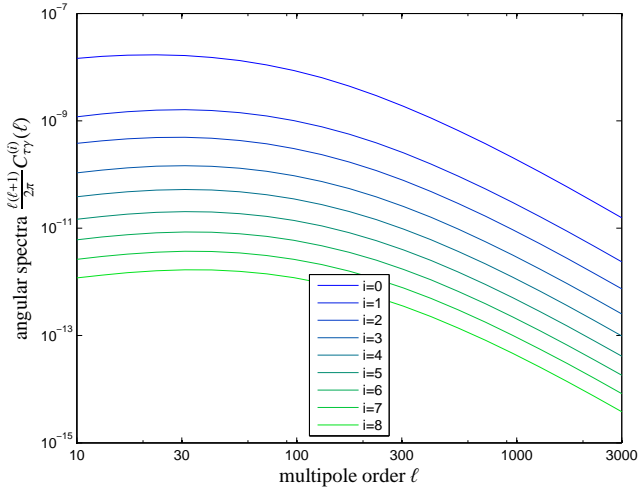


**Figure 5.** Galaxy-iSW cross-spectra  $C_{\tau\gamma}^{(i)}(\ell)$ ,  $i = 0 \dots 8$ , weighted with orthogonal polynomials  $p_i(\chi)$ , as a function of the multipole order  $\ell$ .  $C_{\tau\gamma}^{(0)}(\ell)$  (blue) refers to the non-tomographic spectrum  $C_{\tau\gamma}(\ell)$ .

ism. Furthermore, we investigate the signal strength of the different spectra and their dependence on the number of polynomials used.

#### 4.1 Variances of galaxy number counts

For forecasting statistical errors, we need to derive expressions for the signal covariance and noise. We will start from a discrete formulation with a set of weighting coefficients  $w_m$  for the counted galaxy number  $m$ . Clearly, the weighting coefficient  $w_m$  will depend on the distance of the respective galaxy. Later, we will generalise the formalism to the continuous case, in which the weighting procedure is performed by the polynomials  $p_i(\chi)$ . The standard deviation  $\sigma_{ww}$  of a weighted galaxy count with weighting coefficients  $w_m$  is given by

$$\sigma_{ww}^2 = \frac{1}{\sum_m w_m \sum_n w_n} \sum_{m,n} w_m w_n \delta_{mn} \quad (27)$$

which reduces to a Poissonian result in the case of  $w_m$  being either 0 or 1:

$$\sigma_{ww}^2 = \frac{1}{\bar{n}} \quad \text{with} \quad \bar{n} = \sum_n w_n. \quad (28)$$

The counted quantity  $\bar{n}$  in our case is defined as the mean density of galaxies per steradian, for which we will substitute  $\bar{n} = 40/\text{arcmin}^2$ , which is characteristic for the EUCLID galaxy survey. Considering two different sets of weighting factors  $w_m$  and  $v_n$ , we generalise the standard deviation to

$$\sigma_{wv}^2 = \frac{1}{\sum_m w_m \sum_n v_n} \sum_m w_m v_m, \quad (29)$$

which will in the continuum limit be a cross variance weighted with two different polynomials. For the continuum limit the transition

$$\sum_m \dots \rightarrow \bar{n} \int d\chi n(\chi) \dots \quad (30)$$

is performed which conserves the total number count  $\bar{n}$  due to the unit normalised galaxy distribution function  $n(\chi)$ . The discrete weighting sets  $w_m$  and  $v_n$  are then represented by  $p_i(\chi)$  and  $p_j(\chi)$  so that the noise covariance in the continuous case reads

$$N_{\gamma\gamma}^{(ij)}(\ell) \equiv \sigma_{ij}^2 = \frac{1}{\bar{n}} \frac{\int d\chi n(\chi) p_i(\chi) p_j(\chi)}{\int d\chi n(\chi) p_i(\chi) \int d\chi n(\chi) p_j(\chi)}. \quad (31)$$

The noise term  $N_{\gamma\gamma}^{(ij)}(\ell)$  still depends on  $\ell$  since the polynomials are constructed for each multipole order separately. We omit the  $\ell$ -dependence of the polynomials  $p_i(\chi)$  for clarity. Eqn. (31) motivates the following choice of normalisation for our polynomials:

$$p_i(\chi) \leftarrow \frac{p_i(\chi)}{\int d\chi n(\chi) p_i(\chi)}. \quad (32)$$

In this normalisation the galaxy number noise reads

$$N_{\gamma\gamma}^{(ij)}(\ell) = \frac{1}{\bar{n}} \int d\chi n(\chi) p_i(\chi) p_j(\chi), \quad (33)$$

while the galaxy spectrum can be written as

$$S_{\gamma\gamma}^{(ij)}(\ell) = \int_0^{\chi_H} \frac{d\chi}{\chi^2} W_{\gamma}^{(i)}(\chi) W_{\gamma}^{(j)}(\chi) P(k = \ell/\chi) \quad (34)$$

The limitation in polynomial order due to increasing noise in the polynomials  $p_i(\chi)$  can already be illustrated: Since  $n(\chi)$  is a slowly varying function the rapid oscillations of high order polynomials will drive the values of the integrals  $\int d\chi n(\chi) p_i(\chi)$  to smaller numbers and will therefore increase the noise in  $p_i(\chi)$ . We point out that for order zero the non-tomographic case is recovered, giving the standard Poissonian expression for the noise  $N_{00} = 1/\bar{n}$  and the integrated galaxy spectrum in the signal part  $S_{\gamma\gamma}^{(00)}(\ell) = S_{\gamma\gamma}(\ell)$ .

While the orthogonalisation procedure leads to a diagonal galaxy signal covariance, the noise part will not be diagonal any more:  $N_{\gamma\gamma}^{(ij)} \neq 0$  for  $i \neq j$ . In contrary to this method, a traditional binning in  $z$  would lead to a diagonal noise contribution and off-diagonals in the signal part.

#### 4.2 Fisher analysis

In order to use both iSW signals and galaxy spectra in our Fisher analysis, we now define an extended data vector

$$\mathbf{x}(\ell) = \begin{pmatrix} \tau(\ell) \\ \gamma^{(i)}(\ell) \end{pmatrix}. \quad (35)$$

The total covariance matrix,  $C(\ell) = S(\ell) + N(\ell)$ , for these data vectors is block-diagonal due to the independence of the  $\ell$ -modes: Each block

$$C(\ell) = \begin{pmatrix} C_{\tau\tau}(\ell) & C_{\tau\gamma}^{(j)}(\ell) \\ C_{\tau\gamma}^{(i)}(\ell) & C_{\gamma\gamma}^{(ij)}(\ell) \end{pmatrix} \quad (36)$$

consists of a signal part

$$S(\ell) = \begin{pmatrix} S_{\tau\tau}(\ell) & C_{\tau\gamma}^{(j)}(\ell) \\ C_{\tau\gamma}^{(i)}(\ell) & S_{\gamma\gamma}^{(ij)}(\ell) \end{pmatrix}, \quad (37)$$

where  $S_{\gamma\gamma}^{(ij)}(\ell) \propto \delta_{ij}$  by construction, and a noise contribution

$$N(\ell) = \begin{pmatrix} N_{\tau\tau}(\ell) & 0 \\ 0 & N_{\gamma\gamma}^{(ij)}(\ell) \end{pmatrix}. \quad (38)$$

with polynomial orders  $0 \leq i, j \leq q$ . Due to uncorrelated noise in the CMB and the galaxy density field the noise of the cross-spectra vanishes. The CMB part consists of the pure iSW signal

$$S_{\tau\tau}(\ell) = \int_0^{\chi_H} \frac{d\chi}{\chi^2} W_\tau^2(\chi) P_{\delta\delta}(k = \ell/\chi) \quad (39)$$

with  $P_{\delta\delta}(k) = P_{\delta\delta}/(\chi H k)^4$  while the noise can be split into the primary CMB fluctuations  $C_{\text{CMB}}(\ell)$  and an instrumental noise term  $C_{\text{beam}}(\ell)$  of PLANCK (Planck Collaboration et al. 2011):

$$N_{\tau\tau}(\ell) = C_{\text{CMB}}(\ell) + w^{-1} \exp(-\Delta\theta^2 \ell^2), \quad (40)$$

with the beam size  $\Delta\theta = 8.77 \times 10^{-4}$  and the squared pixel noise  $w^{-1} = 0.2 \mu\text{K}/T_{\text{CMB}}$  (Knox 1995). The noiseless cross spectra are formed by one modified weighting function only:

$$C_{\tau\gamma}^{(i)}(\ell) = \int_0^{\chi_H} \frac{d\chi}{\chi^2} W_\tau(\chi) W_\gamma^{(i)}(\chi) P_{\delta\delta}(k = \ell/\chi) \quad (41)$$

with  $P_{\delta\delta}(k) = P_{\delta\delta}/(k\chi H)^2$ . We point out that only the galaxy part of the signal covariance was diagonalised by our method. Consequently, the cross-spectra  $C_{\tau\gamma}^{(i)}(\ell)$  are the only off-diagonal entries in the covariance matrix.

The likelihood for observing these Gaussian-distributed modes  $\mathbf{x}(\ell)$  for a given parameter set  $\mathbf{p}$  is defined as (Tegmark, 1997):

$$\mathcal{L}(\mathbf{x}(\ell) | \mathbf{p}) = \frac{1}{\sqrt{(2\pi)^N \det C(\ell)}} \exp\left(-\frac{1}{2} \mathbf{x}^T(\ell) C^{-1}(\ell) \mathbf{x}^*(\ell)\right). \quad (42)$$

Defining the data matrix as  $D_{ij}(\ell) = x_i(\ell) x_j^*(\ell)$  with  $\langle D \rangle = C$  and using the relation,  $\ln \det(C) = \text{tr} \ln(C)$  one can write the  $\chi^2$ -functional  $\mathcal{L} \propto \exp(-\chi^2/2)$ , with help of the logarithmic likelihood  $L \equiv -\ln \mathcal{L}$ :

$$\chi^2 = -2L = \text{tr} \sum_\ell \left[ \ln C + C^{-1} D \right]. \quad (43)$$

Each multipole  $\ell$  provides  $(2\ell + 1)$  independent  $m$ -modes. If we interpret  $\mathcal{L}$  as a Bayesian probability, the local behaviour of the likelihood function around the point of maximum likelihood is determined by the Hesse matrix of  $L$  at this point:

$$(C^{-1})_{\mu\nu} \equiv \frac{\partial^2 L}{\partial p_\mu \partial p_\nu} \quad (44)$$

The Fisher information matrix is then given as the expectation value of this quantity summed over all multipole orders  $\ell$ :

$$F_{\mu\nu} = \left\langle \frac{\partial^2 L}{\partial p_\mu \partial p_\nu} \right\rangle = \sum_\ell \frac{2\ell + 1}{2} \text{tr} \left( \frac{\partial}{\partial p_\mu} \ln C(\ell) \frac{\partial}{\partial p_\nu} \ln C(\ell) \right). \quad (45)$$

For each  $\ell$  the  $(2\ell + 1)/2$   $m$ -modes provide statistically independent information. In the course of our Fisher matrix calculations

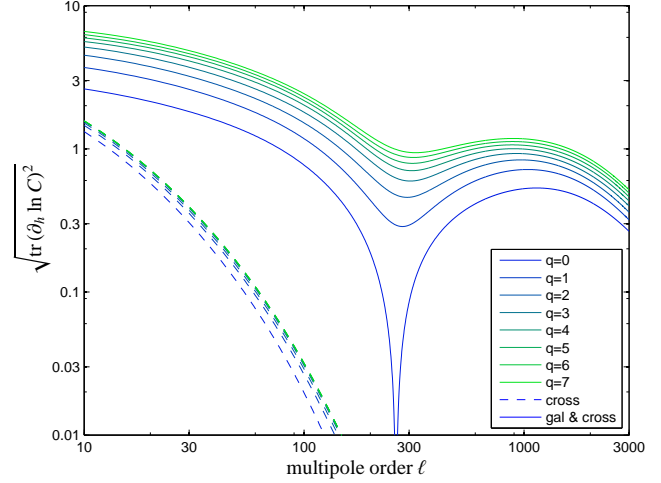


**Figure 6.** Sensitivity  $\sqrt{\text{tr}(\partial_h \ln C(\ell))^2}$  of the Fisher matrix with respect to the Hubble parameter  $h$  as a function of the multipole order  $\ell$ , and cumulative polynomial order  $q$ . Sensitivities are shown with derivatives of all spectra taken into account (solid lines) in comparison to the case where only the cross-spectra were considered in the signal part (dashed lines). For the covariance the survey properties of EUCLID have been assumed.

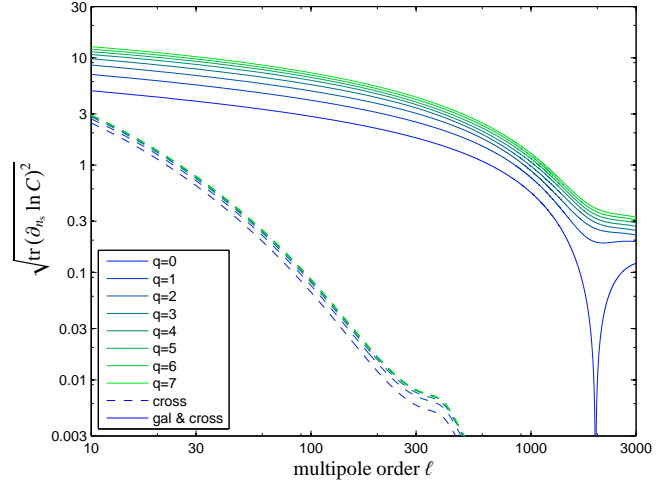


**Figure 7.** Sensitivity  $\sqrt{\text{tr}(\partial_{n_s} \ln C(\ell))^2}$  of the Fisher matrix with respect to the initial slope of the power spectrum  $n_s$  as a function of the multipole order  $\ell$ , and cumulative polynomial order  $q$ . Sensitivities are shown with derivatives of all spectra taken into account (solid lines) in comparison to the case where only the cross-spectra were considered in the signal part (dashed lines). For the covariance the survey properties of EUCLID have been assumed.

we will work in the limit  $\partial S_{ij}/\partial p_\mu \gg \partial N_{ij}/\partial p_\mu$  and therefore neglect the noise dependence on the cosmological parameters. This approximation is well justified in our case.

Next we have a look at the ratio of the sensitivities of the spectra with respect to cosmological parameters and the covariance. This quantity equals the contribution of a certain multipole  $\ell$  to the respective Fisher matrix diagonal element:

$$\sqrt{\text{tr} \left( \frac{\partial \ln C(\ell)}{\partial p_\mu} \right)^2} = \sqrt{\frac{2}{2\ell + 1} \frac{dF_{\mu\mu}}{d\ell}}. \quad (46)$$

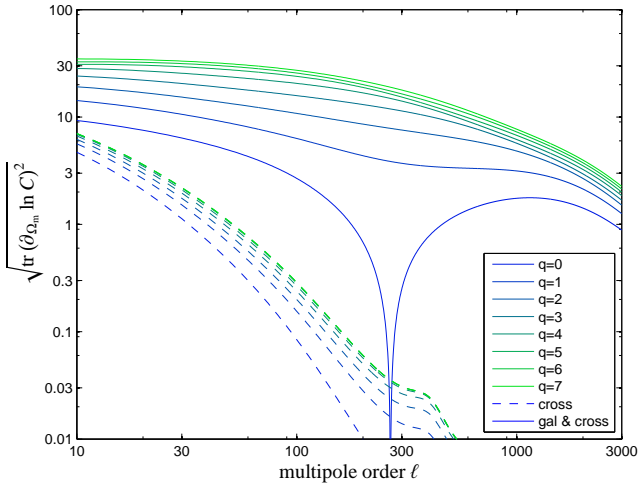


**Figure 8.** Sensitivity  $\sqrt{\text{tr}(\partial_{\Omega_m} \ln C(\ell))^2}$  of the Fisher matrix with respect to the matter density parameter  $\Omega_m$  as a function of the multipole order  $\ell$ , and cumulative polynomial order  $q$ . Sensitivities are shown with derivatives of all spectra taken into account (solid lines) in comparison to the case where only the cross-spectra were considered in the signal part (dashed lines). For the covariance the survey properties of EUCLID have been assumed.

In Fig. 6 - Fig. 8 we show these sensitivities in solid lines for the full information from galaxy spectra, cross-spectra and iSW-effect included for the parameters  $h$ ,  $n_s$  and  $\Omega_m$ , respectively. At zero order they all exhibit a certain  $\ell$ -range at which the covariance is insensitive to variations of the respective cosmological parameter. Naturally, angular scales in the vicinity of this zero point do not contribute much sensitivity to the Fisher matrix. This effect is cured if we include all polynomials  $0 \leq i \leq q$ . The combination of multiple line of sight-weighted measurements lifts the sensitivities at these points continuously with increasing number of involved polynomials until the effect saturates.

For multipole orders  $\ell$  reaching higher values ( $\ell \approx 3000$ ) the sensitivity starts to drop rapidly. On these small scales the noise contribution begins to dominate and the Fisher matrix ceases to grow further.

In dashed lines the sensitivities are shown if only the cross-spectra are included in the derivatives. Again the sensitivities grow with increasing cumulative polynomial order  $q$ , although in this case the zero order sensitivity does not suffer from any singular effects. Characteristic properties of the iSW-effect are recovered showing it to be a large scale effect due to the  $k^{-2}$  proportionality originating in the Poisson equation. Above multipoles of about  $l \approx 100$  the information provided by the cross spectra becomes negligible. Clearly, the cross-spectra Fisher matrix is most sensitive to the matter density parameter  $\Omega_m$ , which shows the strongest increase in sensitivity for increasing cumulative polynomial order  $q$ .

### 4.3 Signal to noise ratio

A signal's power to constrain cosmological parameters is most reliably quantified by the signal to noise ratio

$$\Sigma^2 = f_{\text{sky}} \sum_{\ell} \frac{2\ell+1}{2} \text{tr}(C^{-1}(\ell) S(\ell))^2. \quad (47)$$

Besides the physical process the signal to noise ratio strongly depends on the characteristics of the survey at hand. In the case of

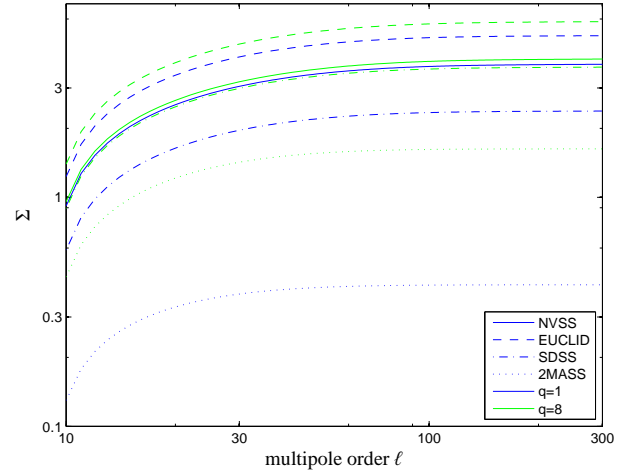


**Figure 9.** Cumulative signal to noise ratio  $\Sigma$  depending on the multipole-order  $\ell$  for the survey characteristics of 2MASS (dotted), SDSS (dashed-dotted), EUCLID (dashed) and NVSS (solid). Shown is the improvement between cumulative polynomial order  $q = 1$  (blue) and  $q = 8$  (green).

galaxy surveys the most important survey parameters are the sky coverage  $f_{\text{sky}}$  and the median redshift  $z_{\text{med}}$ . In Fig 9 the signal to noise ratios for the survey characteristics of EUCLID ( $z_{\text{med}} \approx 0.1$ , Afshordi et al. 2004), SDSS ( $z_{\text{med}} \approx 0.5$ , Bielby et al. 2010) and NVSS ( $z_{\text{med}} \approx 1.2$ , Boughn & Crittenden 2005) are shown. Clearly, also the signal to noise ratio increases for higher polynomial orders due to the diagonal structure of the signal covariance. We find an improvement of  $\approx 16\%$  in the signal to noise ratio between cumulative polynomial order  $q = 1$  and  $q = 8$ . As expected, at a multipole order of a few hundred the cumulative signal strength saturates as a result of the Poissonian  $k^{-2}$  damping term in the iSW-effect. The actual realisation of the matter distribution in the observed universe introduces a systematic noise in the iSW detections known as local variance. Using the so called optimal method one can decrease this bias by working conditional on the large scale structure data and gain 7% in signal to noise ratio (Frommert et al. 2008). The tomographical method presented in our work should be also applicable to the reconstructed large scale structure used in the optimal method. Therefore, a combination of these two methods would be sensible.

### 4.4 Statistical errors

The Cramér-Rao inequality introduces a lower limit on the marginalized standard deviation of the estimated cosmological parameters. These are given by the diagonal elements of the inverse Fisher matrix:

$$\sigma_{\mu} \geq \left( (F^{-1})_{\mu\mu} \right)^{\frac{1}{2}}. \quad (48)$$

In Fig. 10 these errors are depicted for the five cosmological parameters  $\Omega_m$ ,  $\sigma_8$ ,  $h$ ,  $n_s$  and  $w$ . The plot follows the evolution of the errors with increasing number of included polynomials  $q$ . While for small polynomial orders the Cramér-Rao errors decrease rapidly with different characteristics for each parameter, the improvement slows down for higher order polynomials and assumes a characteristic behaviour. This behaviour can approximately be described by the inverse root of the polynomial order  $\sigma_{\mu} \propto 1/\sqrt{q}$ . A simi-

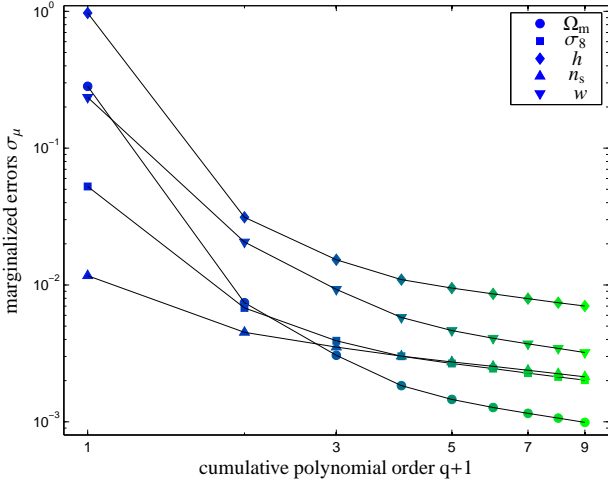


**Figure 10.** Lower limits on the marginalized statistical errors  $\sigma_\mu$  on the estimates of the cosmological parameters  $\Omega_m$  (circles),  $\sigma_8$  (squares),  $h$  (lozenges),  $n_s$  (triangles, pointing up) and  $w$  (triangles, pointing down) derived from the Cramér-Rao inequality, as a function of the cumulative polynomial order  $q$ . The Fisher matrix was derived including the derivatives of all spectra  $C_{\gamma\gamma}^{(i)}(\ell)$ ,  $C_{\tau\gamma}^{(i)}(\ell)$  and  $C_{\tau\tau}(\ell)$ . Again, the EUCLID survey characteristics have been used.

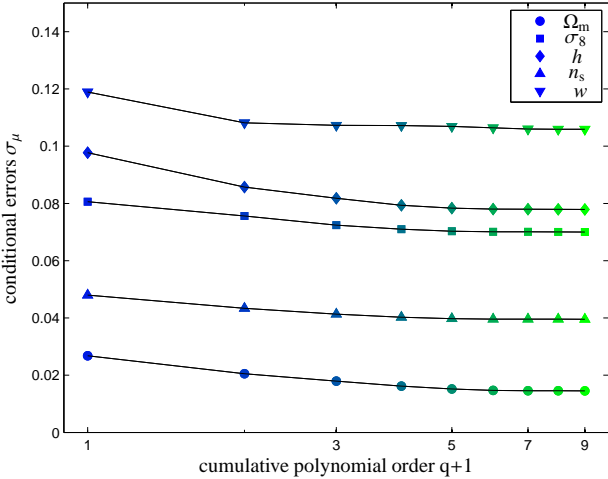


**Figure 11.** Conditional statistical errors  $\sigma_{\mu,\text{con}}$  on the estimates of the cosmological parameters  $\Omega_m$  (circles),  $\sigma_8$  (squares),  $h$  (lozenges),  $n_s$  (triangles, pointing up) and  $w$  (triangles, pointing down). The Fisher matrix was derived including the derivatives of the cross-spectra  $C_{\tau\gamma}^{(i)}(\ell)$  only, EUCLID survey characteristics have been used.

lar characteristic was found in the application of this method to the weak lensing shear spectra (Schäfer & Heisenberg 2011). Clearly, the cosmological parameter  $\Omega_m$  profits most of the tomographic method, which was already indicated by its sensitivity improvement discussed in Section 4.2. Going to even higher orders is difficult due to cumulative errors in the Gram-Schmidt orthogonalisation method.

If we are interested in how a single cosmological parameter can be constrained assuming that all other parameters are fixed, we have to study the conditional errors. These can be obtained from the inverse diagonal elements of the Fisher matrix

$$\sigma_{\mu,\text{con}} = (F_{\mu\mu})^{-\frac{1}{2}}. \quad (49)$$

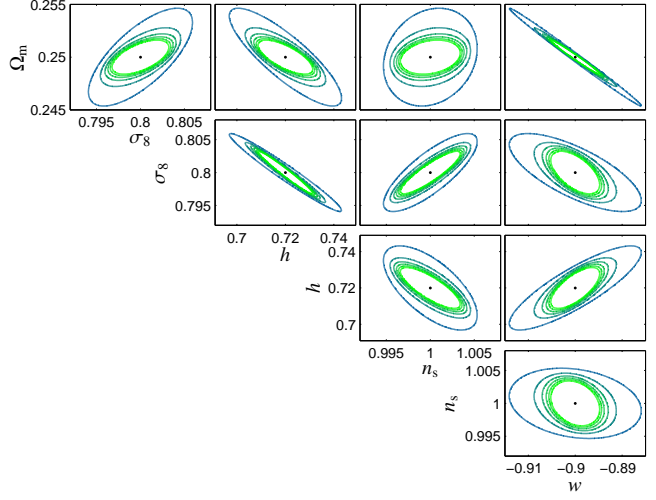


**Figure 12.** The 2-dimensional  $1\sigma$ -error ellipses for the cosmological parameters  $\Omega_m$ ,  $\sigma_8$ ,  $h$ ,  $n_s$  and  $w$  from EUCLID using tomography with orthogonal polynomials are shown in this plot. The  $1\sigma$  confidence regions decrease in size with increasing number of included polynomials, reaching from  $q = 2$  (blue) to  $q = 8$  (green). The ellipses are evaluated with a maximum multipole order of  $\ell_{\text{max}} = 3000$ .

For studying the improvement provided by the cross-spectra, we plot the conditional errors as a function of cumulative polynomial order  $q$  in Fig. 11. Here, only the derivatives of the cross-spectra were taken into account in the Fisher matrix calculation. Again  $\Omega_m$  is subjected to the strongest improvement, its conditional error decreases by  $\approx 30\%$ . In contrast to the marginalized errors the evolution of the conditional errors does not show a  $1/\sqrt{q}$  behaviour but rather saturates at polynomial order of  $q \approx 5$ .

Finally, we are interested in the 2-dimensional marginalized logarithmic likelihood  $\chi_m^2$  around the fiducial model  $\mathbf{p}_{\text{fid}}$

$$\chi_m^2 = \begin{pmatrix} p_\mu - p_{\mu,\text{fid}} \\ p_\nu - p_{\nu,\text{fid}} \end{pmatrix} \begin{pmatrix} (F^{-1})_{\mu\mu} & (F^{-1})_{\mu\nu} \\ (F^{-1})_{\nu\mu} & (F^{-1})_{\nu\nu} \end{pmatrix} \begin{pmatrix} p_\mu - p_{\mu,\text{fid}} \\ p_\nu - p_{\nu,\text{fid}} \end{pmatrix} \quad (50)$$

for which the  $1\sigma$ -error ellipses are depicted in Fig. 12. Starting with  $q = 2$ , we have combined up to nine polynomials. Besides the expected shrinking of the ellipses for higher numbers of included polynomials, it is interesting to see how the degeneracies slightly change their orientations in the course of tomographic improvement. This is very likely due to distance dependencies of the signal sensitivities.

## 5 SUMMARY

In this paper a tomographic method for measuring iSW-galaxy cross-spectra and galaxy spectra has been presented. It has been carried out by sight-weighting of the iSW-effect and the tracer density field with specifically constructed orthogonal polynomials.

(i) The Gram-Schmidt orthogonalisation procedure has been used to construct orthogonal polynomials in order to diagonalise the weighted galaxy signal covariance. The method projects out statistically independent signal contributions at the price of off-diagonals in the noise part. It differs from traditional tomographical approaches, for instance from most tomographical techniques in weak lensing measurements, in which the noise part is diagonalised. Due to cumulative numerical errors with increasing polynomial order, this method is limited to order  $i \approx 8$ .



(ii) The improvement of the signal to noise ratios with cumulative polynomial order was investigated for the galaxy surveys 2MASS (Afshordi et al. 2004), SDSS (Bielby et al. 2010), NVSS (Boughn & Crittenden 2005) and EUCLID. The signal to noise ratio for the cross-spectra only has been improved by 16% at a cumulative polynomial order of  $q = 8$ .

(iii) A Fisher-matrix analysis was used to forecast how well cosmological parameters can be constrained by different galaxy surveys, combining signals from the iSW-effect as well as from the tracer density field. The marginalised errors show simple inverse square-root behaviour with increasing number of included polynomials, which can be interpreted also as a sign of the statistical independent signal contributions. Conditional errors on parameters constrained only by the cross-spectra decrease by up to  $\approx 30\%$  in case of the matter density parameter  $\Omega_m$ .

(iv) While for the cross-spectra only the conditional errors show a saturation already at quite low number of included polynomials  $q \approx 5$ , it would still be worth improving this method in order to reach even higher orders, since marginalised errors for the full signal did not yet saturate at cumulative order of  $q = 8$ .

(v) Using the wrong model in the construction of the polynomials can introduce an estimation bias on cosmological parameters. This effect was thoroughly studied in a similar approach for weak lensing measurements (Schaefer & Heisenberg 2011). In most cases the bias was found to be small compared to the statistical errors. Since, in addition, iteration between parameter estimation and polynomial construction is able to further reduce this bias, a wrongly chosen cosmology appears unlikely to affect measurements.

## ACKNOWLEDGEMENTS

Our work was supported by the German Research Foundation (DFG) within the framework of the Priority Programme 1177 and the excellence initiative through the Heidelberg Graduate School of Fundamental Physics. We also thank Patricio Vielva and Carlos Hernández-Monteagudo for suggesting to compare the signal to noise ratios for different contemporary galaxy surveys.

## REFERENCES

- Abramowitz M., Stegun I. A., 1972, Handbook of Mathematical Functions
- Afshordi N., Loh Y.-S., Strauss M. A., 2004, Phys. Rev. D, 69, 083524
- Aghanim N., Majumdar S., Silk J., 2008, Reports on Progress in Physics, 71, 066902
- Bardeen J. M., Bond J. R., Kaiser N., Szalay A. S., 1986, ApJ, 304, 15
- Bartelmann M., Schneider P., 2001, Physics Reports, 340, 291
- Bielby R., Shanks T., Sawangwit U., Croom S. M., Ross N. P., Wake D. A., 2010, MNRAS, 403, 1261
- Boughn S., Crittenden R., 2004, Nature, 427, 45
- Boughn S. P., Crittenden R. G., 2005, MNRAS, 360, 1013
- Boughn S. P., Crittenden R. G., Turok N. G., 1998, New Astronomy, 3, 275
- Crittenden R. G., Turok N., 1996, Physical Review Letters, 76, 575
- Fixsen D. J., 2009, ApJ, 707, 916
- Frommert M., Ensslin T. A., Kitaura F. S., 2008, MNRAS, 391, 1315
- Fry J. N., 1996, ApJL, 461, L65
- Giannantonio T., Scranton R., Crittenden R. G., Nichol R. C., Boughn S. P., Myers A. D., Richards G. T., 2008, Phys. Rev. D, 77, 123520
- Ho S., Hirata C. M., Padmanabhan N., Seljak U., Bahcall N., 2008, Phys.Rev.D, 78:043519,2008
- Knox L., 1995, Phys. Rev. D, 52, 4307
- Limber D. N., 1953, ApJ, 117, 134
- Linder E. V., Jenkins A., 2003, MNRAS, 346, 573
- Lue A., Scoccimarro R., Starkman G., 2004, Phys. Rev. D, 69, 044005
- Lumsden S. L., Heavens A. F., Peacock J. A., 1989, MNRAS, 238, 293
- McEwen J. D., Vielva P., Hobson M. P., Martínez-González E., Lasenby A. N., 2007, MNRAS, 376, 1211
- Mo H. J., Jing Y. P., White S. D. M., 2007
- Ostriker J. P., Vishniac E. T., 1986, ApJL, 306, L51
- Planck Collaboration Ade P. A. R., Aghanim N., Arnaud M., Ashdown M., Aumont J., Baccigalupi C., Baker M., Balbi A., Banday A. J., 2011, A&A, 536, A1
- Sachs R. K., Wolfe A. M., 1967, ApJ, 147, 73
- Schaefer B. M., Heisenberg L., 2011, ArXiv e-prints 1107.2213
- Sheth R. K., Mo H. J., Tormen G., 2001, MNRAS, 323, 1
- Smail I., Hogg D. W., Blandford R., Cohen J. G., Edge A. C., Djorgovski S. G., 1995, MNRAS, 277, 1
- Spergel D. N., Verde L., Peiris H. V., Komatsu E., Nolte M. R., Bennett C. L., Halpern M., Hinshaw G., Jarosik N., Kogut A., Limon M., Meyer S. S., Page L., Tucker G. S., Weiland J. L., Wollack E., Wright E. L., 2003, ApJS, 148, 175
- Sugiyama N., 1995, ApJS, 100, 281
- Tegmark M., Peebles P. J. E., 1998, ApJL, 500, L79
- Turner M. S., White M., 1997, Phys. Rev. D, 56, 4439
- Vielva P., Martínez-González E., Tucci M., 2006, MNRAS, 365, 891
- Wang L., Steinhardt P. J., 1998, ApJ, 508, 483
- Zeldovich Y. B., Sunyaev S. R. A., 1980, Pis ma Astronomicheskii Zhurnal, 6, 737
- Zhang P., 2006, Phys. Rev. D, 73, 123504

This paper has been typeset from a  $\text{\TeX}/\text{\LaTeX}$  file prepared by the author.